PCCP

RSC Publishing

PAPER

View Article Online
View Journal | View Issue

Cite this: *Phys. Chem. Chem. Phys.*, 2013, **15**, 12734

Specific interactions between the quaternary ammonium oligoether-based ionic liquid and water as a function of pressure

Hai-Chou Chang,*[a] Jyh-Chiang Jiang,*[b] Tsai-Yi Chen,[a] Hsing-Sheng Wang,[a] Leo Yuxiu Li,[a] Wei-Wen Hung[a] and Sheng Hsien Lin[c]

Received 3rd April 2013,
Accepted 30th May 2013

DOI: 10.1039/c3cp51396c

www.rsc.org/pccp

The interactions between Ammoeng 100 and water are probed using high-pressure infrared measurements and DFT-calculations. The results of infrared absorption profiles suggest that the energetically favored approach for water molecules to interact with Ammoeng 100 is *via* the formation of anion–water interactions, whereas the alkyl C–H groups play much less important roles. After comparison with pure Ammoeng 100, it appears that no appreciable changes in band frequencies of alkyl C–H vibrations occurred as Ammoeng 100 was mixed with D_2O. The presence of D_2O has a red-shift effect on the peak frequency of the S═O stretching vibration under the pressures below 1 GPa in comparison to the absorption frequencies of pure Ammoeng 100. This observation is likely related to local structures of the S═O groups interacting with D_2O molecules. DFT-calculations indicate that the most energetically favored conformation of ion pairs should be the species having only one hydrophilic hydrogen bonding. The results of calculations reveal that water addition may induce the partial replacement of C–H···O interactions with strong hydrogen bonding between anions and water molecules.

Introduction

Ionic liquids are typically composed of bulky organic cations and anions with a melting temperature below 100 °C. Their extraordinary properties such as nonvolatile nature and liquid state in a broad temperature range make them attractive alternatives to volatile organic solvents for many innovative applications.[1–3] Although ionic liquids are environmentally green solvents compared to traditional organic solvents, the high viscosity of ionic liquids has restricted their use as solvents in technical applications such as heat-transfer fluids. To expand the application of ionic liquids, addition of a suitable co-solvent to an ionic liquid has come into focus in recent years.[4–13] The study of ionic liquid-based mixtures becomes more and more attractive in recent years and this is one of the motivations for the current work.[1–13]

The properties of ionic liquid-based mixtures are very complex that have been shown using experimental and theoretical methods. Generally, the structures and properties of these ionic systems are mainly dominated by the electrostatic interactions.[2,5] Based on previous studies, ionic liquids differ from the classical salts at least in one aspect: they possess hydrogen bonds that induce structural directions.[2,5] However, the role of hydrogen bonding in ionic liquids is still an issue of debate in the literature.[5,14] The local structures and self-assembly of ionic liquid–water mixtures have been studied, while the physical properties are key features for the applications of ionic liquids. At high ionic liquid concentrations, ionic liquids seem to form clusters, as in the pure state, and water molecules interact with the clusters without interacting among themselves. Ionic liquids containing dissolved water may not be regarded as homogeneous solvents but have to be considered as microheterogeneous materials, where the microheterogeneity may be attributed to incomplete mixing at the molecular level.[15–18]

Because ionic liquids are entirely composed of ions, ionic liquids have been utilized in the preparation of ion gels (a new class of solid state electrolytes).[19–22] The addition of gelling agents to ionic liquids occasionally leads to the gelation of ionic liquids and the gelling agents include low molecular weight gelators, nanoparticles, and block copolymers. Such ion gels, prepared by chemical or physical gelation, frequently exhibit intriguing properties (*e.g.*, high ionic conductivity, quasi-solidification, and flexibility) making

[a] *Department of Chemistry, National Dong Hwa University, Shoufeng, Hualien 974, Taiwan. E-mail: hcchang@mail.ndhu.edu.tw*
[b] *Department of Chemical Engineering, National Taiwan University of Science and Technology, Taipei 106, Taiwan. E-mail: jcjiang@mail.ntust.edu.tw*
[c] *Department of Applied Chemistry, National Chiao Tung University, Hsinchu 30010, Taiwan*

them attractive for the application of ion gels. However, the preparation of ion gels suffers from the diverse limitations of expensive synthetic procedures and unknown potential toxicity. Developing new gelation methods for ionic liquids is crucial for the significant application of ion gels. There has recently been much interest in using water to prepare ion gels and this inexpensive approach yields ion gels with good physical and mechanical properties.[6,7] Recently the gelation of the quaternary ammonium oligoether-based ionic liquid Ammoeng 100 with water has been addressed.[6,7] Nevertheless, the local structures of water-based ion gels are not clear at present. In this work, we use variable pressure as a window into the hydrogen bonding structures in Ammoeng 100–water mixtures.

Knowledge of the nature of hydrogen bonding interactions is fundamental to understand the physical properties of ionic liquids. The hydrogen bonding interactions are complex for ionic liquid–water mixtures with varying anions, due to pronounced anion–water interactions. The molecular state of water absorbed from air in ionic liquids has been studied using vibrational spectroscopy, which indicates that water molecules interact with the anions and exist in symmetric 1 : 2 type hydrogen-bonded complexes.[23,24] Many research studies of ionic liquid mixtures are interested in the interactions between water and anions, while the interactions of water with cations have been studied limitedly. Water miscibility of ionic liquids is affected by the length of alkyl side-chains and the role of water in ionic liquids is closely related to the supramolecular structures of ionic liquids. Researchers have demonstrated that small amounts of water in ionic liquids have a dramatic effect on the rate of diffusion.[17] Based on the theoretical results of Voth's group,[15] at high ionic liquid concentration ionic liquids seem to form clusters, as in the pure state, and water molecules interact with the clusters without interacting among themselves. In the present investigation, our intent is to achieve further understanding of aggregation properties in ionic liquid–water mixtures.

Various spectroscopic and theoretical studies have been made to probe the structures, interactions, and solvation of ionic liquid-based systems.[1–5] Previous studies on the structures of ionic liquids have included the use of X-ray crystallography.[1] Although the results of crystal structures are highly informative on the relative geometry changes, crystallography does not provide direct information on the local structures in the liquid state. Thus, vibrational spectroscopy (IR or Raman) is often used to explore hydrogen bonded structures of liquid mixtures. Generally, vibrational studies were performed at ambient pressure and mostly at room temperature. Recently interest in pressure as an experimental variable has been growing in physicochemical studies.[21,22,25–27] Under high-pressure conditions, the relative weights of the strong intramolecular interactions responsible for molecular bonding and of the weaker intermolecular forces defining the aggregation states are altered. In this study, we show that high-pressure infrared spectroscopy is a sensitive method to probe the structural organization in ionic liquid–water mixtures.

Experimental section

Samples were prepared using Ammoeng 100 (>95%, UniRegion Bio-Tech) and D_2O (99.9 atom% D, Aldrich). A diamond anvil cell (DAC) of Merrill–Bassett design, having a diamond culet size of 0.6 mm, was used for generating pressures up to *ca.* 2 GPa. Two type-IIa diamonds were used for mid-infrared measurements. The sample was contained in a 0.3 mm-diameter hole in a 0.25 mm-thick inconel gasket mounted on the diamond anvil cell. To reduce the absorbance of the samples, CaF_2 crystals (prepared from a CaF_2 optical window) were placed into the hole and compressed firmly prior to inserting the sample. A droplet of a sample filled the empty space of the entire hole of the gasket in the DAC, which was subsequently sealed when the opposed anvils were pushed toward one another. Infrared spectra of the samples were measured on a Perkin-Elmer Fourier transform spectrophotometer (model Spectrum RXI) equipped with a LITA (lithium tantalite) mid-infrared detector. The infrared beam was condensed through a 5× beam condenser onto the sample in the diamond anvil cell. Typically, we chose a resolution of 4 cm^{-1} (data point resolution of 2 cm^{-1}). For each spectrum, typically 1000 scans were compiled. To remove the absorption of the diamond anvils, the absorption spectra of DAC were measured first and subtracted from those of the samples. Pressure calibration follows Wong's method.[28,29] The pressure dependence of screw on moving distances was measured.

Results and discussion

The quaternary ammonium-based ionic liquid chosen for the preparation of the mixture in this article is Ammoeng 100, as shown in Fig. 1. In general, Ammoeng ionic liquids have amphiphilic structures containing both long alkyl chains and hydroxyl groups. Fig. 2 displays infrared spectra of pure Ammoeng 100 obtained under ambient pressure (curve a) and

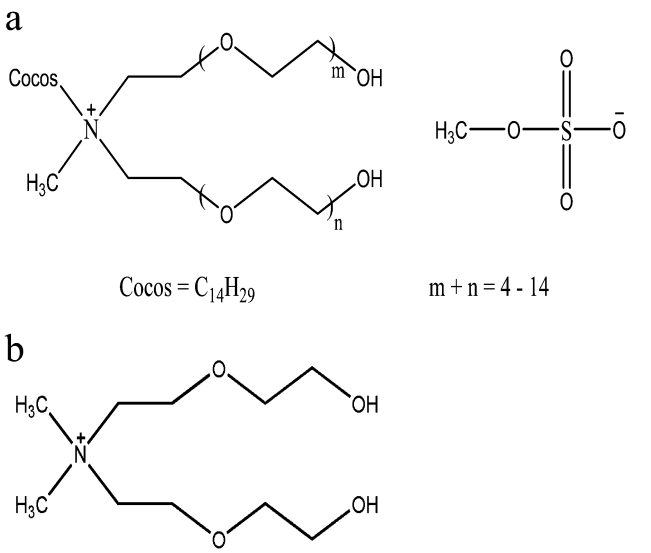

Fig. 1 Chemical structures of (a) Ammoeng 100 and (b) the cation used in the DFT-calculation.

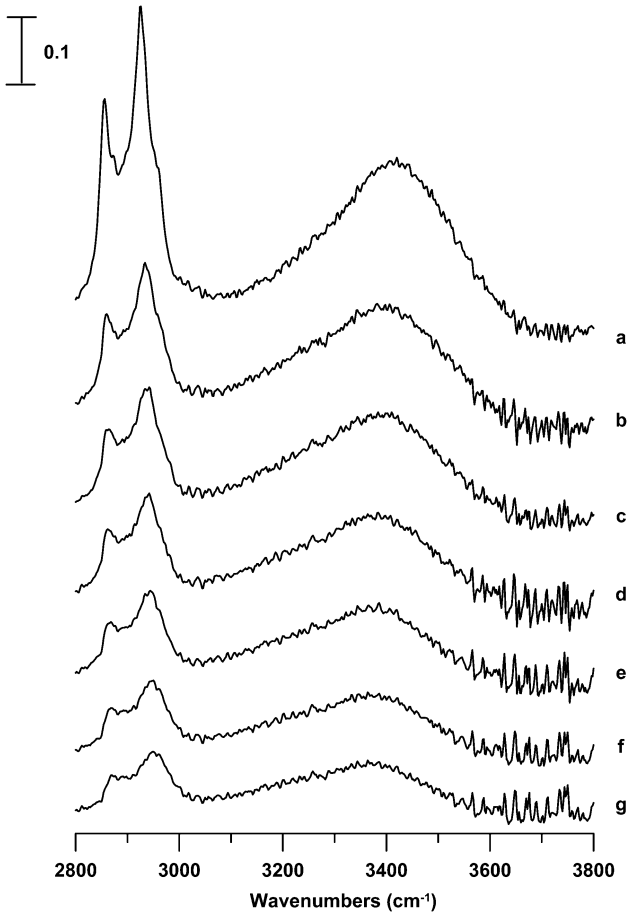

Fig. 2 IR spectra of pure Ammoeng 100 obtained under ambient pressure (curve a) and at 0.3 (curve b), 0.9 (curve c), 1.5 (curve d), 1.9 (curve e), 2.3 (curve f), and 2.5 GPa (curve g).

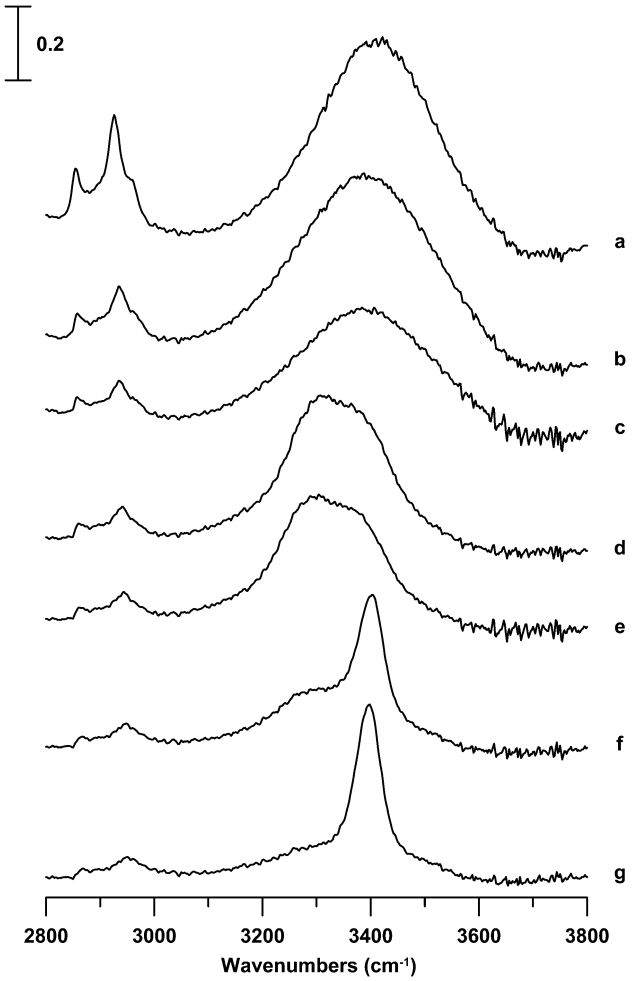

Fig. 3 IR spectra of an Ammoeng 100–D_2O mixture (10 wt% Ammoeng 100) obtained under ambient pressure (curve a) and at 0.3 (curve b), 0.9 (curve c), 1.5 (curve d), 1.9 (curve e), 2.3 (curve f), and 2.5 GPa (curve g).

at 0.3 (curve b), 0.9 (curve c), 1.5 (curve d), 1.9 (curve e), 2.3 (curve f), and 2.5 GPa (curve g). We have concentrated our analysis on the 2800–3800 cm^{-1} region which contains the C–H and O–H stretching modes, Fig. 2.[21,22] The infrared spectrum exhibits two discernible peaks, *i.e.*, at 2857 and 2926 cm^{-1}, respectively, corresponding to C–H stretching modes of the alkyl groups, Fig. 2a. The broad band at *ca.* 3401 cm^{-1} in Fig. 2a can be assigned to hydrogen bonded O–H stretching modes.[30] As the sample was compressed, *i.e.*, increasing from ambient (Fig. 2a) to 0.3 GPa (Fig. 2b), alkyl C–H bands were blue shifted to 2863 and 2935 cm^{-1}, respectively, Fig. 2b. The blue shift may originate from the combined effect of the overlap repulsion enhanced by hydrostatic pressure, C–H···O contacts, and so forth.[21,22,31–33] Nevertheless, the red shift of the O–H band at *ca.* 3374 cm^{-1} is obvious as the pressure was elevated, Fig. 2b. This behavior is in accord with the general trend observed for a red shift with pressure for O–H and C═O stretching modes in strongly hydrogen bonded O–H···O and C═O···H systems, respectively.[30] In contrast to strong hydrogen bonding, the C–H covalent bond tends to blue-shift as a result of formation of a weak hydrogen bond.

Fig. 3 presents infrared spectra of an Ammoeng 100–D_2O mixture (10 wt% Ammoeng 100) obtained under ambient pressure (curve a) and at 0.3 (curve b), 0.9 (curve c), 1.5 (curve d), 1.9 (curve e), 2.3 (curve f), and 2.5 GPa (curve g). The C–H stretching absorptions overlap with the O–H stretching bands of H_2O, so D_2O was used in this study. By comparing Fig. 2a and 3a, we observe no appreciable changes in C–H spectral features in the presence of D_2O under ambient pressure, Fig. 3a. The broad absorption band at *ca.* 3406 cm^{-1} revealed in Fig. 3a is mainly attributed to the hydrogen bonded O–H stretching modes of the diluted HOD in the Ammoeng 100–D_2O mixture. The HOD molecules may mainly originate from the H–D exchange from D_2O to the cation. HOD is also a typical impurity existing in D_2O. As the pressure was elevated to 0.3 GPa, the red shift of the hydrogen bonded O–H band is obvious, Fig. 3b. At a pressure of 1.5 GPa (Fig. 3d), the O–H spectral features show further evolution through an observation of bandwidth narrowing. This observation indicates that a pressure-induced phase transition occurs, Fig. 3d. At room temperature, compression of liquid water leads to tetragonal ice VI at pressure above 1.05 GPa and further to cubic ice VII above 2.1 GPa.[30] The sharper O–H features, Fig. 3d–g, may correspond to the high order environment in ice-like structures.[30] The IR spectra of both ice VI (Fig. 3d–e) and ice VII (Fig. 3f–g) consist of two O–H bands

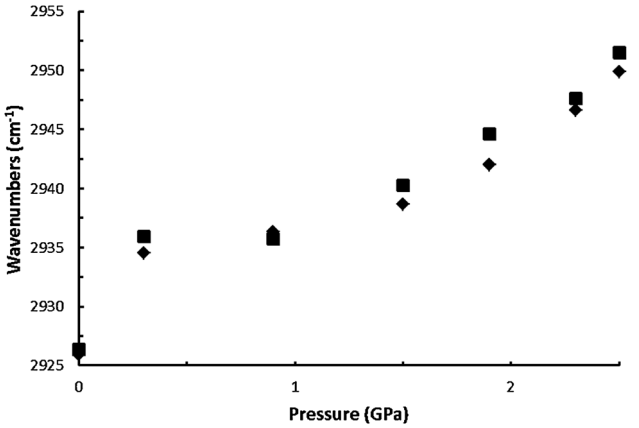

Fig. 4 Pressure dependence of the C–H stretching frequencies of pure Ammoeng 100 (diamonds) and the Ammoeng 100–D_2O mixture (squares).

overlapping each other. These two bands become well separated in the derivative spectra. As shown in Fig. 3b–g, the compression leads to blue frequency shifts of the C–H stretching modes.

The absorption frequencies of the dominant alkyl C–H band at about 2926 cm^{-1} are plotted *versus* pressures in Fig. 4, while we notice that the alkyl C–H band in Fig. 4 displays anomalous non-monotonic pressure-induced frequency shifts. For pure Ammoeng 100, the compression leads to blue frequency shifts at the pressure below 0.3 GPa, then no appreciable changes in the band frequency (*cf.* Fig. 2b–c), and then blue-shifts again upon further increasing the pressure (*cf.* Fig. 2d–g). This discontinuity in frequency shift, Fig. 4, is in agreement with the trends revealed in our previous studies.[34] The alkyl C–H band frequency of pure Ammoeng 100 increases significantly at 0.3 GPa, Fig. 4, and this may indicate a pressure-induced solidification (or structural transformation) at a pressure of 0.3 GPa. A structural reorganization or second phase transition may take place at pressures above 1 GPa as revealed in Fig. 4. After comparison with pure Ammoeng 100, it appears that no appreciable changes in band frequencies of alkyl C–H vibrations occurred as Ammoeng 100 was mixed with D_2O, Fig. 4. Our results in Fig. 4 suggest that the presence of D_2O does not perturb the ionic liquid–ionic liquid clustering (phase transition or cross-linking) in the non-polar region at the pressure of 0.3 GPa. The role of water in ionic liquids is complex and depends on the supramolecular structures of ionic liquids.[15–17] We would like to point out that the HOD molecules in the Ammoeng 100–D_2O mixture are still liquid-like under the pressure of 0.3–1 GPa as revealed in Fig. 3b and c. Thus, the Ammoeng 100–D_2O mixture, Fig. 3b and c may behave like gel due to the pressure-induced transition *via* a three-dimensional cross-linked network within the liquid D_2O. Our results indicate that high pressure can be applied to tune the relative weights of ionic liquid aggregation states in the Ammoeng 100–D_2O mixture even in the liquid (or gel) state.

In order to gain further insights into the local structures of ionic liquids, the pressure dependencies of S═O stretching vibration of pure Ammoeng 100 and Ammoeng 100–D_2O are presented in Fig. 5 and 6, respectively. Fig. 5 displays infrared

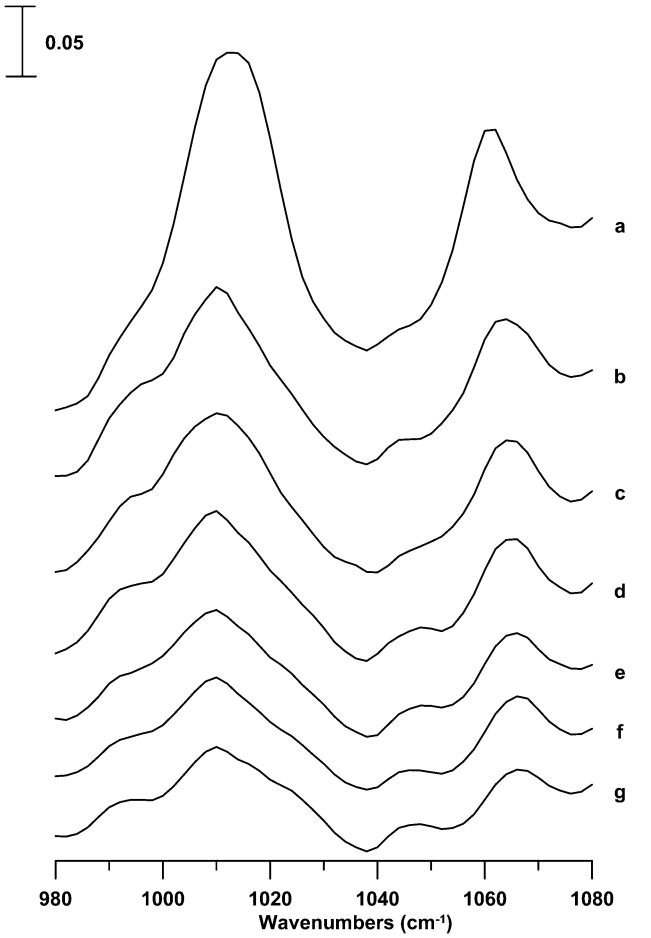

Fig. 5 IR spectra of pure Ammoeng 100 obtained under ambient pressure (curve a) and at 0.3 (curve b), 0.9 (curve c), 1.5 (curve d), 1.9 (curve e), 2.3 (curve f), and 2.5 GPa (curve g).

spectra of pure Ammoeng 100 obtained under ambient pressure (curve a) and at 0.3 (curve b), 0.9 (curve c), 1.5 (curve d), 1.9 (curve e), 2.3 (curve f), and 2.5 GPa (curve g) in the 980–1080 cm^{-1} region. As revealed in Fig. 5a, the symmetric SO_3 stretch appears at 1013 cm^{-1} under ambient pressure.[35,36] The symmetric SO_3 stretch shows a red shift to 1011 cm^{-1} upon compression, Fig. 5b and this result represents the weakening of the S═O bond. The sharper S═O structure revealed in Fig. 5b is in part due to the higher order and anisotropic environment in a solid structure. As the sample was compressed, *i.e.*, increasing the pressure from 0.3 GPa (Fig. 5b) to 2.3 GPa (Fig. 5e), no appreciable changes in the band frequency of the S═O stretching absorption were observed.

Fig. 6 displays infrared spectra of an Ammoeng 100–D_2O mixture (10 wt% Ammoeng 100) obtained under ambient pressure (curve a) and at 0.3 (curve b), 0.9 (curve c), 1.5 (curve d), 1.9 (curve e), 2.3 (curve f), and 2.5 GPa (curve g) in the 980–1080 cm^{-1} region. A red shift in band frequency of the S═O stretching vibration from 1013 cm^{-1} (Fig. 5a) to 1006 cm^{-1} (Fig. 6a) occurred as the ionic liquid was diluted by D_2O under ambient pressure. This result is remarkably different from what is revealed for the alkyl C–H groups, Fig. 3a. The S═O stretching mode underwent a

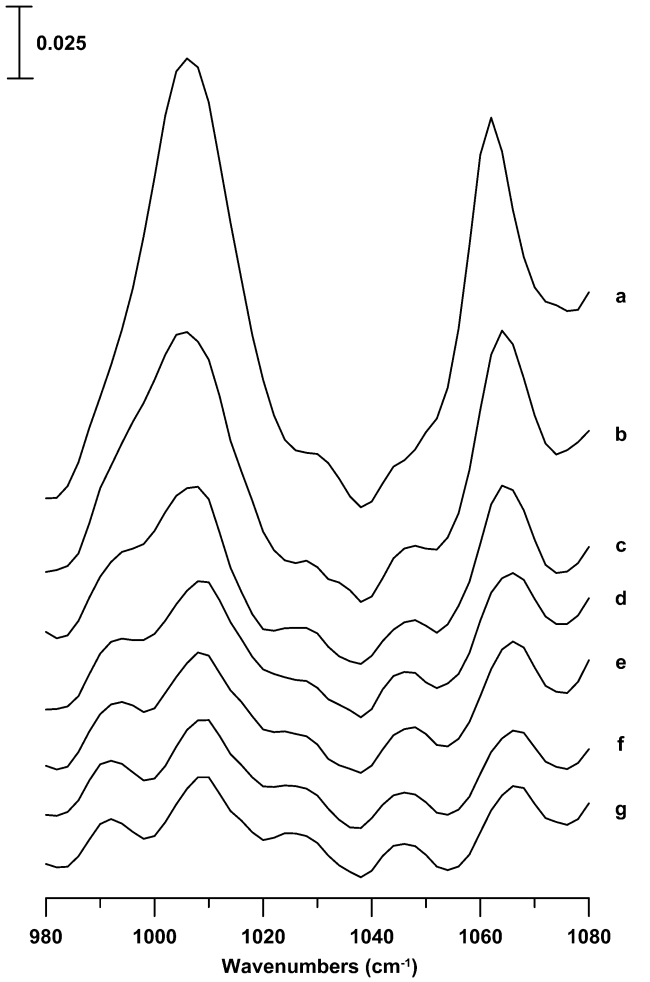

Fig. 6 IR spectra of an Ammoeng 100–D_2O mixture (10 wt% Ammoeng 100) obtained under ambient pressure (curve a) and at 0.3 (curve b), 0.9 (curve c), 1.5 (curve d), 1.9 (curve e), 2.3 (curve f), and 2.5 GPa (curve g).

red-shift in frequency as D_2O was added, Fig. 6a, but no significant changes in C–H stretching frequency were observed in Fig. 3a under ambient pressure. Previous studies have shown that the frequency shifts of the vibration modes are closely related to changes in the hydration states and the liquid structures.[34] Our results may suggest that the energetically favored approach for the D_2O molecules to interact with Ammoeng 100 is *via* the formation of anion–D_2O interactions. The compression leads to a red shift in frequency of the S═O stretching vibration to 1004 cm^{-1}, Fig. 6b, while blue-shifts in frequency of the S═O stretching vibration are observed for further compressions, Fig. 6c–g. Looking into more detail in Fig. 6d–g, the spectral features of the S═O stretching vibration of the Ammoeng 100–D_2O mixture show further evolution upon dilution through the observation of decreases in band widths in comparison to the S═O absorption bandwidths of pure Ammoeng 100 as revealed in Fig. 5d–g. Our results indicate that the S═O absorption bandwidths in Fig. 5 and 6 are more concentration-sensitive than the alkyl C–H bandwidths as shown in Fig. 2 and 3. A possible explanation for this effect is the hydrogen bonding formation between the S═O groups and D_2O. The high order ice-like O–D structures may be one of the reasons to yield the bandwidth narrowing, Fig. 6d–g. This observation suggests the formation of a certain ice-like structure around the S═O groups, but the details remain unclear. Based on our results, the S═O groups seem to be more favorable sites for hydrogen bonding than the alkyl groups. We also observed several C–O stretching bands in the 1020–1080 cm^{-1} region. One of the C–O peaks locating between 1020 and 1030 cm^{-1} becomes obvious, Fig. 6 (in comparison to Fig. 5), due to the bandwidth narrowing of S═O absorption.

To illustrate the frequency shift, the absorption frequencies of the S═O stretching vibration was presented *versus* pressures in Fig. 7 and the S═O stretching band displays anomalous non-monotonic pressure-induced frequency shifts. As shown in Fig. 7, the presence of D_2O has a red-shift effect on the peak frequency of the S═O stretching vibration under the pressures below 1 GPa in comparison to the absorption frequencies of pure Ammoeng 100. This observation is likely related to local structures of the S═O groups interacting with D_2O molecules. We note that simple density effects may result in monotonic frequency shifts due to increased density upon compression. In other words, the non-monotonic frequency shifts observed in this study suggest the changes in structures due to hydrogen bonding. The red-shifts of S═O stretches may be due to the replacement of an interaction between the anion and a cation with an interaction with D_2O. We note that the S═O absorption peaks of the Ammoeng 100–D_2O mixture show the trend of an initial red shift followed by blue shifting under compression, Fig. 7. As pure Ammoeng 100 and the Ammoeng 100–D_2O mixture were compressed to the pressures above 1 GPa, Fig. 7, the symmetric SO_3 absorption displays almost the same band frequencies and the presence of D_2O does not have a drastic effect on the band frequencies of S═O stretches as the Ammoeng 100 was diluted by D_2O. This result is remarkably different from the lower SO_3 frequency observed for the Ammoeng 100–D_2O mixture under the pressures below 1 GPa, Fig. 7. This behavior may arise from changes in water-cluster

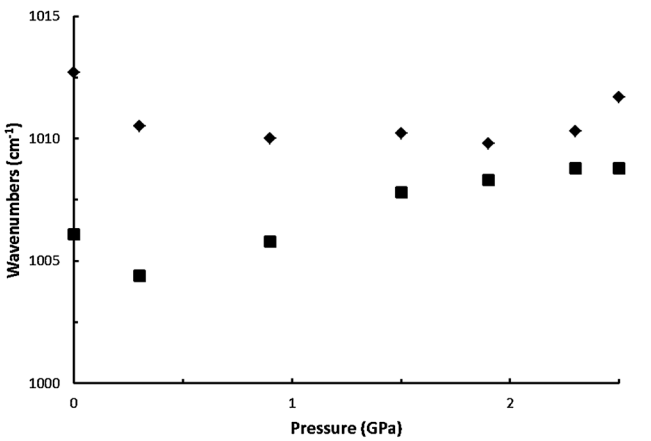

Fig. 7 Pressure dependence of the symmetric SO_3 stretching frequencies of pure Ammoeng 100 (diamonds) and the Ammoeng 100–D_2O mixture (squares).

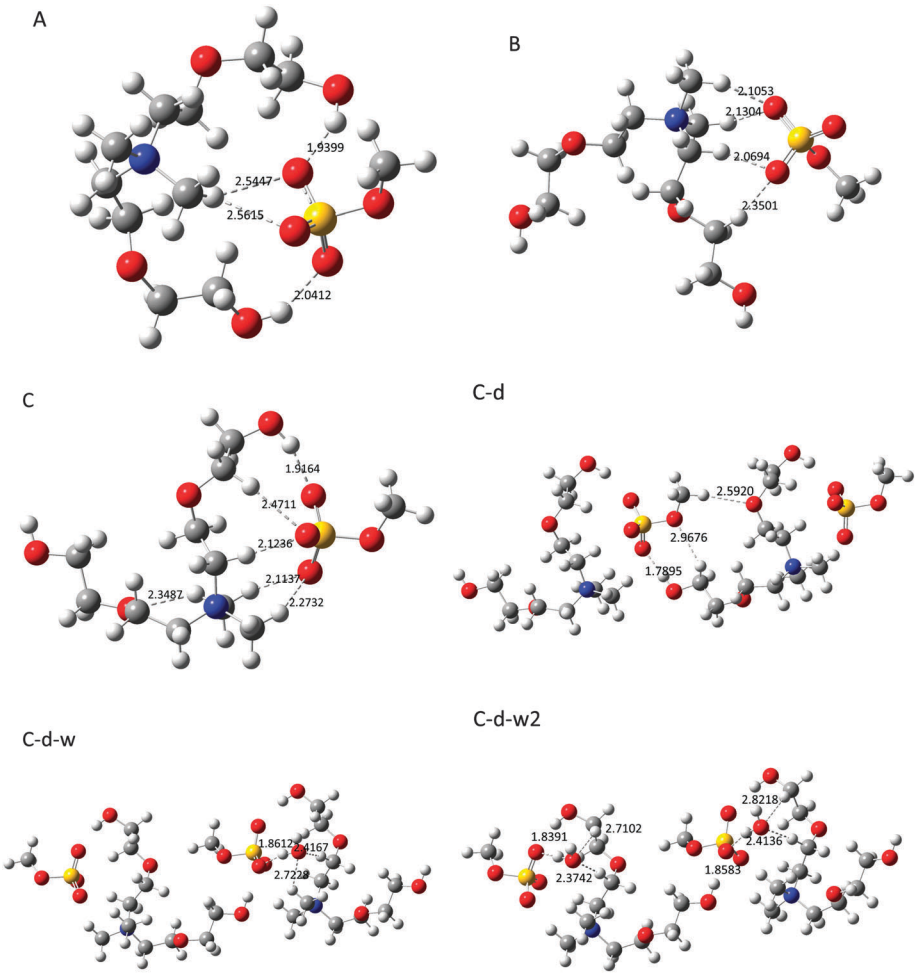

Fig. 8 Optimized structures of ion pairs (species A, B, and C), the ion-pair dimer (species C-d), ion-pair-(water) (species C-d-w), and ion-pair-(water)$_2$ (species C-d-w2).

sizes (ice-like structures) and a perturbation in the geometrical properties of hydrogen-bond network as the pressure is elevated to above 1 GPa. The association of water molecules to form the ice-like structures may induce the clustering of Ammoeng 100. In the literature, the researchers have reported that the cation–anion interaction can be distinguished from anion–water or cation–water interactions using vibrational spectroscopy,[37] and ionic liquid–water mixtures are not an unstructured homogeneous solution.[38]

To develop further insight into the hydration mechanism, we have performed density functional theory (DFT) calculations using the Gaussian program package.[39] As compared with the chemical structure of Ammoeng 100, Fig. 1a, we choose the shorter side-chain cation, having two methyl groups and two side-chains with $m = n = 1$, in our calculations (see Fig. 1b). Fig. 8 displays the DFT-calculated structures of [cation][anion] ion pairs (species A, B, and C), ([cation][anion])$_2$ ion-pair dimer (species C-d), ([cation][anion])$_2$(water) (species C-d-w), and ([cation][anion])$_2$(water)$_2$ (species C-d-w2). The geometry optimization was calculated by using the B3LYP level with 6-31+G*. Table 1 displays energy results and predicted symmetric SO_3 stretching frequencies. As illustrated in Fig. 8A and B, the approach for the anion ($CH_3SO_4^-$) to interact with the cation is through the formation of two hydrophilic hydrogen bonds (–O–H···O═S–) for species A and hydrophobic interactions (–C–H···O═S–) for species B. Based on calculated results revealed in Table 1, the hydrophilic conformer (species A) is more stable in thermodynamic energy than the hydrophobic conformer (species B). Nevertheless, Table 1 indicates that the most energetically favored conformation of ion pairs should be species C having only one hydrophilic hydrogen bonding (–O–H···O═S–). This fact suggests the non-negligible role of weak hydrogen bonds such as C–H···O interactions in the structures of ion pairs.

Table 1 DFT-calculated relative energies (hartree mol^{-1}) and symmetric SO_3 stretching frequencies (cm^{-1})[a]

Species[a]	Relative energies	Calcd frequency
A	−1489.637914	979.9
B	−1489.636111	985.0
C	−1489.645719	992.0
C-d	−2979.307899	988.4, 992.0
C-d-w	−3055.722625	985.4, 991.8
C-d-w2	−3132.137958	985.0, 986.8

[a] Structures illustrated in Fig. 8.

It appears that charge-enhanced alkyl C–H···O interactions somehow provide complementary stabilization energies to provide stability to the local structures of neat ionic liquids.

As the clusters increase in size, the number of low-lying isomers increases exponentially and the structure identification is complicated. Thus, we only extend the structure of species C to develop the structure of the ion-pair dimer (species C-d), dimer-water (species C-d-w), and dimer-$(water)_2$ (species C-d-w2), Fig. 8. As revealed in the structures of species C-d-w and C-d-w2, water addition disrupts C–H···O interactions between the cation and the anion. It was known that the addition of an appropriate amount of water to Ammoeng 100 results in the formation of ionogel, but the detailed mechanism is still not clear. Based on our calculations of species C-d-w and C-d-w2, the gelation of Ammoeng 100/water may involve the partial replacement of C–H···O interactions with strong hydrogen bonding between the anion and water molecules. Table 1 displays the frequencies of two symmetric SO_3 stretching vibrations located at 988.4 and 992.0 cm^{-1} for species C-d and the symmetric SO_3 stretching bands are red-shifted to 985.4 and 991.8 cm^{-1} for species C-d-w. As species C-d is coordinated to two water molecules, the symmetric SO_3 stretching bands are further red-shifted to 985.0 and 986.8 cm^{-1} for species C-d-w2. This result is in agreement with the red-shift observed upon dilution under ambient pressure, Fig. 7.

Conclusion

The pressure-dependent infrared spectral features indicate that the alkyl C–H bands of Ammoeng 100 display non-monotonic pressure-induced frequency shifts. The compression leads to blue frequency shifts at the pressure below 0.3 GPa, then no appreciable changes in the band frequency, and then blue-shifts again upon further increasing the pressures. No significant changes in alkyl C–H stretching frequencies were observed as Ammoeng 100 was mixed with D_2O. This observation suggests that the presence of D_2O does not perturb the ionic liquid–ionic liquid association in the non-polar region. In contrast to the C–H groups, the S═O stretching modes underwent red-shift in frequency in the presence of D_2O under the pressures below 1 GPa. Our results suggest that the energetically favored approach for D_2O molecules to interact with Ammoeng 100 is *via* anion–D_2O interactions. DFT-calculations indicate the non-negligible role of hydrophobic interactions (C–H···O) in the structures of ion pairs. Water addition disrupts C–H···O interactions and the partial replacement of hydrophobic interaction with strong hydrogen bonding between anion and water molecules occurs in Ammoeng 100–water mixtures.

Acknowledgements

The authors thank the National Dong Hwa University and the National Science Council (Contract No. NSC 101-2113-M-259-006-MY3) of Taiwan for financial support. The authors thank Yu-Sheng Cheng and Rong-Lin Zhang for the assistance.

Notes and references

1 *Ionic Liquids in Synthesis*, ed. P. Wasserscheid and T. Welton, Wiley VCH, Weinheim, Germany, 2008.
2 J. Dupont and J. D. Scholten, *Chem. Soc. Rev.*, 2010, **39**, 1780.
3 E. W. Castner and J. F. Wishart, *J. Chem. Phys.*, 2010, **132**, 120901.
4 M. Brehm, H. Weber, A. S. Pensado, A. Stark and B. Kirchner, *Phys. Chem. Chem. Phys.*, 2012, **14**, 5030.
5 A. Wulf, K. Fumino and R. Ludwig, *Angew. Chem., Int. Ed.*, 2010, **49**, 449.
6 J. C. Ribot, C. Guerrero-Sanchez, R. Hoogenboom and U. S. Schubert, *J. Mater. Chem.*, 2010, **20**, 8279.
7 P. Reddy, K. J. Chiyen, N. Deenadayalu and D. Ramjugernath, *J. Chem. Thermodyn.*, 2011, **43**, 1178.
8 S. Sarkar, R. Pramanik, C. Ghatak, P. Setua and N. Sarkar, *J. Phys. Chem. B*, 2010, **114**, 2779.
9 Q. G. Zhang, N. N. Wang and Z. W. Yu, *J. Phys. Chem. B*, 2010, **114**, 4747.
10 K. S. Rao, T. Singh, T. J. Trivedi and A. Kumar, *J. Phys. Chem. B*, 2011, **115**, 13847.
11 P. K. Nayak, A. P. Hathorne and H. Bermudez, *Phys. Chem. Chem. Phys.*, 2013, **15**, 1806.
12 Y. Fukaya and H. Ohno, *Phys. Chem. Chem. Phys.*, 2013, **15**, 4066.
13 W. Shi, K. Damodaran, H. B. Nulwala and D. R. Luebke, *Phys. Chem. Chem. Phys.*, 2012, **14**, 15897.
14 K. Fumino, T. Peppel, M. Geppert-Rybczynska, D. H. Zaitsau, J. K. Lehmann, S. P. Verevkin, M. Kockerling and R. Ludwig, *Phys. Chem. Chem. Phys.*, 2011, **13**, 14064.
15 Y. Wang and G. A. Voth, *J. Phys. Chem. B*, 2006, **110**, 18601.
16 J. N. A. C. Lopes and A. A. H. Padua, *J. Phys. Chem. B*, 2006, **110**, 3330.
17 U. Schroder, J. D. Wadhawan, R. G. Compton, F. Marken, P. A. Z. Suarez, C. S. Consorti, R. F. de Souza and J. Dupont, *New J. Chem.*, 2000, **24**, 1009.
18 M. Tanaka, T. Yago and M. Wakasa, *Phys. Chem. Chem. Phys.*, 2013, **15**, 787.
19 H. Park, H. S. Kim and Y. M. Jung, *J. Phys. Chem. B*, 2011, **115**, 1743.
20 S. Taguchi, T. Matsumoto, T. Ichikawa, T. Kato and H. Ohno, *Chem. Commun.*, 2011, **47**, 11342.
21 H. C. Chang, T. C. Hung, S. C. Chang, J. C. Jiang and S. H. Lin, *J. Phys. Chem. C*, 2011, **115**, 11962.
22 H. C. Chang, S. C. Chang, T. C. Hung, J. C. Jiang, J. L. Kuo and S. H. Lin, *J. Phys. Chem. C*, 2011, **115**, 23778.
23 M. Lopez-Pastor, M. J. Ayora-Canada, M. Valcarcel and B. Lendl, *J. Phys. Chem. B*, 2006, **110**, 10896.
24 L. Cammarata, S. G. Kazarian, P. A. Salter and T. Welton, *Phys. Chem. Chem. Phys.*, 2001, **3**, 5192.
25 J. C. Jiang, K. H. Lin, S. C. Li, P. M. Shih, K. C. Hung, S. H. Lin and H. C. Chang, *J. Chem. Phys.*, 2011, **134**, 044506.
26 H. C. Chang, T. C. Hung, H. S. Wang and T. Y. Chen, *AIP Adv.*, 2013, **3**, 032147.

27 Y. Umebayashi, J. C. Jiang, K. H. Lin, Y. L. Shan, K. Fujii, S. Seki, S. Ishiguro, S. H. Lin and H. C. Chang, *J. Chem. Phys.*, 2009, **131**, 234502.
28 P. T. T. Wong, D. J. Moffatt and F. L. Baudais, *Appl. Spectrosc.*, 1985, **39**, 733.
29 P. T. T. Wong and D. J. Moffatt, *Appl. Spectrosc.*, 1987, **41**, 1070.
30 H. C. Chang, K. H. Huang, Y. L. Yeh and S. H. Lin, *Chem. Phys. Lett.*, 2000, **326**, 93.
31 D. Liu, W. Lei, K. Wang, G. Bao, F. Li, J. Hao, B. Liu, T. Cui, Q. Cui and G. Zou, *J. Phys. Chem. B*, 2009, **113**, 7430.
32 M. Jablonski and A. Sadlej, *Chem. Phys. Lett.*, 2008, **463**, 322.
33 O. Russina, B. Fazio, C. Schmidt and A. Triolo, *Phys. Chem. Chem. Phys.*, 2011, **13**, 12067.
34 H. C. Chang, J. C. Jiang, W. C. Tsai, G. C. Chen and S. H. Lin, *J. Phys. Chem. B*, 2006, **110**, 3302.
35 Y. Miller, G. M. Chaban, J. Zhou, K. R. Asmis, D. M. Neumark and R. B. Gerber, *J. Chem. Phys.*, 2007, **127**, 094305.
36 T. Iwahashi, T. Miyamae, K. Kanai, K. Seki, D. Lim and Y. Ouchi, *J. Phys. Chem. B*, 2008, **112**, 11936.
37 P. Stange, K. Fumino and R. Ludwig, *Angew. Chem., Int. Ed.*, 2013, **52**, 2990.
38 R. Hayes, S. Imberti, G. G. Warr and R. Atkin, *Angew. Chem., Int. Ed.*, 2012, **51**, 7468.
39 M. J. Frisch, G. W. Trucks, H. B. Schlegel, G. E. Scuseria, M. A. Robb, J. R. Cheeseman, G. Scalmani, V. Barone, B. Mennucci, G. A. Petersson, H. Nakatsuji, M. Caricato, X. Li, H. P. Hratchian, A. F. Izmaylov, J. Bloino, G. Zheng, J. L. Sonnenberg, M. Hada, M. Ehara, K. Toyota, R. Fukuda, J. Hasegawa, M. Ishida, T. Nakajima, Y. Honda, O. Kitao, H. Nakai, T. Vreven, J. A. Montgomery Jr., J. E. Peralta, F. Ogliaro, M. Bearpark, J. J. Heyd, E. Brothers, K. N. Kudin, V. N. Staroverov, R. Kobayashi, J. Normand, K. Raghavachari, A. Rendell, J. C. Burant, S. S. Iyengar, J. Tomasi, M. Cossi, N. Rega, J. M. Millam, M. Klene, J. E. Knox, J. B. Cross, V. Bakken, C. Adamo, J. Jaramillo, R. Gomperts, R. E. Stratmann, O. Yazyev, A. J. Austin, R. Cammi, C. Pomelli, J. W. Ochterski, R. L. Martin, K. Morokuma, V. G. Zakrzewski, G. A. Voth, P. Salvador, J. J. Dannenberg, S. Dapprich, A. D. Daniels, Ö. Farkas, J. B. Foresman, J. V. Ortiz, J. Cioslowski and D. J. Fox, *Gaussian 09, Revision A.1*, Gaussian, Inc., Wallingford, CT, 2009.